Nonlinear Model Predictive Control Design for Active Cell Balancing and Thermal Management

Muhammad Rizwan Azam[1], Afaq Ahmed[1], Ali Arshad Uppal[1] and Qadeer Ahmed[2]

***Abstract*— Active cell balancing and thermal management are essential for optimizing the performance and extending the lifespan of a battery pack. The battery pack consists of two adjacent $LiFePO_4$ cells connected in series with a bidirectional buck-boost converter. The cell model integrates the electrical and thermal dynamics to form a coupled electro-thermal model. A high-fidelity model is employed to calculate the mean balancing currents and the power losses of an active cell balancing network (ACBN). A nonlinear model predictive controller (NMPC) is designed to minimize SoC imbalances, thermal deviations, and power losses within the ACBN. The CasADi toolbox and the interior point optimizer (Ipopt) algorithm are used to solve the control scheme. The NMPC maintains the SoC difference within a 2% threshold despite the modeling uncertainties and a generic current profile. The inclusion of thermal constraints within the NMPC's cost function ensures that cell temperatures remain within safe operational limits, thereby accommodating temperature variation among cells. The simulations demonstrate the critical role of incorporating thermal dynamics into the NMPC formulation, highlighting the trade-offs between balancing speed, power losses, and thermal management.**

I. Introduction

The integration of series and parallel cell configurations in electric vehicle (EV) battery packs is essential to meet different power and voltage requirements. However, series connections are prone to cell-to-cell imbalances, causing gradual degradation of battery performance [1]. To address this issue, passive and active cell equalization strategies are employed. The passive equalization strategy is a dissipative approach. However, the active equalization methods utilize power electronics circuits-based non-dissipative approaches, e.g., switched capacitor, buck-boost, and flyback converters. The active cell balancing methods facilitate charge transfer between cells, thus enhancing efficiency and lifespan [2], [3].

State-of-charge (SoC) equalization is preferred for cell balancing over terminal voltage for cell balancing due to its direct impact on uniformity and overall pack efficiency [4]. In the literature, extensive efforts are carried out in SoC equalization to meet diverse requirements in EVs and other domains. For instance, cell-to-cell equalization through a bidirectional Cuk converter is explored in [5], employing sequential quadratic programming (SQP) based optimization technique to reduce balancing currents and SoC differences.

Active cell balancing has also been applied to extend the driving range of EVs, initially through reachability analysis [6] and subsequently enhanced by nonlinear model predictive control (NMPC) techniques [1], [7]. The authors in [4] solve a multi-objective optimal control problem to improve the balancing while minimizing power loss via NMPC. Adaptive MPC strategies are also designed to address terminal voltage discrepancies, as demonstrated in [8]. Cell balancing for range enhancement employing three distinct NMPC strategies is detailed in [3].

Various articles in the literature also focus on thermal management along with the active cell balancing objective. In [9], a convex optimization approach addresses cell equalization, thermal management, and voltage stabilization, simultaneously. The authors in [10] discuss a multi-objective control approach to include virtual resistance control for dynamic compensation of terminal voltage variations, thermal management for uniform temperature distribution, and onboard diagnosis for fault detection. [11] utilizes a multi-objective optimization problem for a hierarchical cell balancing strategy, designed to optimize cell equalization while minimizing balancing time and temperature. The SQP based optimal control methodology in [5] is improved in [12] with the integration of thermal dynamics to maintain cell current and temperature within suitable ranges. While various studies have explored the integration of thermal dynamics within the context of cell balancing and optimization strategies, the adoption of a closed-loop MPC-based framework for the thermal management of battery pack has not been extensively investigated.

In recent years, cell electrochemical models have also been utilized for nonlinear optimal control in active cell balancing applications. The research work in [2] introduces a single particle model incorporating electrolyte and temperature dynamics (SPMeT) for an NMPC problem aimed at minimizing conflicting costs effectively. Similarly, [13] applies an SPM model coupled with aging and thermal dynamics for a nonlinear optimal control problem focused on achieving fast charging with minimal battery degradation. While many efforts have been made toward employing accurate cell models, comprehensive network modeling often remains overlooked. As highlighted in one of our previous works in [14], the performance of an ACBN is significantly affected by both static and dynamic network parameters.

In our earlier work [15], we carried out comprehensive mathematical modeling for mean balancing currents and power losses of the ACBN, taking into account the effect of static and dynamic parameters. However, simple electrical dynamics were considered for the Li-ion cells. This research extends the previous work by integrating cell thermal dynamics with ACBN and cell electrical dynamics. This integration aims to not only equalize SoC levels but also manage the thermal behavior of cells, ensuring operational safety and efficiency under a wide range of real-world conditions. The ACBN implemented in the current research work includes a bi-directional buck-boost converter and a battery pack consisting of two series-connected Li-ion cells. A first-order nonlinear equivalent circuit model (ECM) is employed to capture cell electrical dynamics. An NMPC is designed to determine optimal duty cycles for the buck-boost converter, aiming for SoC level equalization and thermal management.

The rest of the paper is organized as follows. The ACBN and cell modeling is presented in section II, which is followed by NMPC design in section III. The discussion of the results is presented in section IV, and the paper is concluded in section V.

II. Mathematical Modeling of Active Cell Balancing Network

Figure 1 shows the interaction of the ACBN with the power train and EV. ACBN is comprised of a buckboost converter and a battery pack consisting of two series connected cells. The pair of MOSFET Q_1 and diode D_1 transfers the excess charge from Cell-1 to Cell-2, whereas Q_2 and D_1 transfer charge from Cell-2 to Cell-1. The MOSFETs Q_1 and Q_2 are turned on using the control signals u_1 and u_2, respectively.

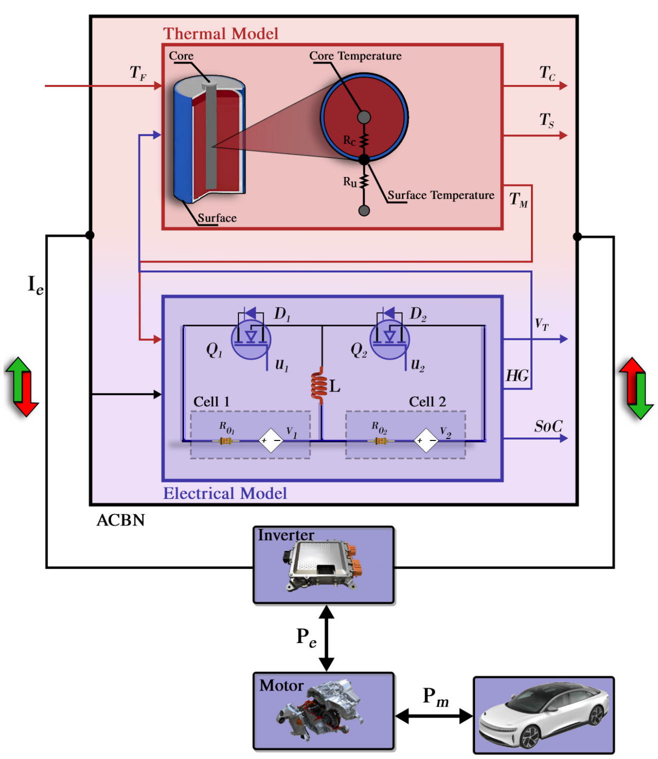

Fig. 1: System level interaction of an EV with ACBN.

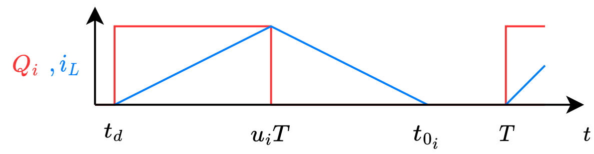

Fig. 2: Piece-wise i_L and switching cycle of Q_i.

A. Mean Balancing Currents in ACBN

Figure 2 shows the switching period of Q_i and corresponding inductor current i_L, which is given as

$$i_L = \begin{cases} 0, & 0 \le t \le t_d \\ \dfrac{v_h}{R_{ch}}\left(1 - e^{\lambda}\right), & t_d \le t \le u_iT \\ e^{\phi_i}\left(I_{p_i} + \dfrac{v_l + V_F}{R_{dis}}\right) - \dfrac{v_l + V_F}{R_{dis}}, & u_iT \le t \le t_{0_i} \\ 0, & t_{0_i} \le t \le T \end{cases}, \quad (1)$$

$$I_{p_i} = \frac{v_h}{R_{ch}}\left(1 - e^{\kappa_i}\right),\ \kappa_i = \frac{t_d - u_iT}{\tau_{ch}},$$

$$t_{0_i} = u_iT + \tau_{dis} ln\left[\frac{R_{dis} v_h}{(v_l + V_F)R_{ch}}\left(1 - e^{\kappa_i}\right) + 1\right],$$

$$\lambda = \frac{t_d - t}{\tau_{ch}},\ \phi_i = \frac{u_iT - t}{\tau_{dis}},\ R_{dis} = R_{0_l} + R_L,$$

$$R_{ch} = R_{0_h} + R_L + R_{ds},\ \tau_{ch} = \frac{L}{R_{ch}},\ \tau_{dis} = \frac{L}{R_{dis}},$$

where $v_h = \max(v_1, v_2)$, $v_l = \min(v_1, v_2)$ and $R_{0_h} = \max(R_{0_1}, R_{0_2}), R_{0_l} = \min(R_{0_1}, R_{0_2})$ represent open circuit voltages (V) and resistances (Ω) of higher and lower SoC cells, respectively; τ_{ch} and τ_{dis} are time constants (s) for charging and discharging paths, respectively; t_0, t_d and T represent time instant at which $i_L = 0$, dead time, and switching time period, respectively; V_F is diode forward voltage drop, duty cycle of Q_i is denoted by u_i, and L represents the inductance of the inductor (H); and R_{ch}, R_{dis}, R_L and R_{ds} represent resistances of charging path, discharging path, cell i, inductor and on-state switching, respectively.

The integration of (1) over the complete switching period yields mean currents for the charging and discharging modes of an inductor

$$I_{ch_i} = \frac{v_h}{TR_{ch}}\left(u_iT - t_d + \tau_{ch}\left(e^{\kappa_i} - 1\right)\right), \quad (2)$$

$$I_{dis_i} = \frac{\tau_{dis}\left(e^{\chi_i} - 1\right)}{T}\left(-I_{p_i} - \frac{a_0(t_{0_i} - u_iT)}{\tau_{dis}\left(e^{\chi_i} - 1\right)} + 1\right), \quad (3)$$

$$\chi_i = \frac{u_iT - t_{0_i}}{\tau_{dis}},\ a_0 = \frac{v_l + V_F}{R_{dis}},$$

where I_{ch} and I_{dis} are mean currents (A) during charging and discharging modes of inductor, respectively, and I_p is the peak inductor current at $t = u_iT$ (cf. figure 2).

B. Power Losses in the Buck-Boost Converter

The power losses due to MOSFETs, on-state resistances of diodes, parasitic resistances of energy storage elements and internal resistances of cells constitute the conduction losses, which are given as

$$
\begin{aligned}
P_{con} &= \sum_{j=1}^{2}\left[\tilde{I}_{ch_j}^2 \tilde{R}_{ch} u_j + \tilde{I}_{dis_j}^2 \tilde{R}_{dis}\left(\frac{t_{0_j} - u_j T}{T}\right)\right] \\
&+ \sum_{j=1}^{2} I_{b_j}^2 R_{0_j}, \qquad (4) \\
\tilde{I}_{ch_j}^2 &= \frac{v_h^2}{TR_{ch}^2}\left[\tau_{ch} e^{\kappa_j}\left(\frac{4-e^{\kappa_j}}{2}\right) + u_j T - t_d - \frac{3}{2}\tau_{ch}\right] \\
\tilde{I}_{dis_j}^2 &= \frac{1}{T}\left[\tau_{dis} I_{p_j}\left(\frac{I_{p_j}}{2} - a_0\right) + a_0^2\left(t_0 - u_j T - \frac{3}{2}\tau_{dis}\right)\right] \\
&+ \frac{1}{T}\left[-\tau_{dis} e^{2\kappa_j}\left(\frac{I_{p_j}^2}{2} + \frac{a_0^2}{2} + a_0 I_{p_j}\right)\right] \\
&+ \frac{1}{T}\left[e^{3\kappa_j} 2 a_0 \tau_{dis}\left(I_{p_j} + a_0\right)\right],
\end{aligned}
$$

where P_{con} represents conduction losses (W); $\tilde{R}_{ch} = R_{ch} - R_{0_h}$, $\tilde{R}_{dis} = R_{dis} - R_{0_l}$; I_{b_j}, cf. (10), (11), is the current of cell-j; and $\tilde{I}_{ch}$ and $\tilde{I}_{dis}$ represent the RMS currents during charging and discharging modes, respectively.

As the buck-boost converter is operated in discontinuous conduction mode, therefore, the switching losses only consider the power losses when MOSFETs are turned off

$$P_{t_f} = \frac{t_f}{2T}\sum_{j=1}^{2} v_h I_{dis_j}, \qquad (5)$$

where t_f is the fall time.

The reverse recovery power loss associated with the body diodes is

$$P_{D_{rr}} = \frac{t_{rr}^2}{2TL}\sum_{j=1}^{2} v_j v_F, \qquad (6)$$

where $P_{D_{rr}}$ and t_{rr} denote the reverse recovery power loss, and time, respectively.

During dead time both Q_1 and Q_2 are off and the inductor discharges through the body diodes, therefore the dead time power losses are characterized as

$$P_{t_d} = \frac{V_F t_d}{2T}\sum_{j=1}^{2} I_{dis_j}, \qquad (7)$$

where P_{t_d} represents dead time power loss and t_d represents the dead time.

C. Coupled Electro-Thermal Model of the Battery Pack

The battery pack consists of two cells connected in series. The electrical dynamics of each cell are modeled using a simple equivalent circuit model (ECM) consisting of the internal resistance (R_{0_i}) and open circuit voltage (v_i) as depicted in figure 1. It is pertinent to mention that the internal resistance R_{0_i} is modeled as a function of SoC and temperature. Moreover, the model integrates the thermal dynamics of cells with the electrical dynamics to form a coupled electro-thermal model. This model captures the core and surface temperatures of a cylindrical battery, employing a two-state thermal model coupled through heat generation and the temperature dependency of electrical parameters. The model simulates the battery's SOC, terminal voltage, and thermal states under diverse operational conditions.

The control-oriented model, reflecting these dynamics, is presented as follows:

$$
\dot{\mathbf{x}} = \mathbf{f}(\mathbf{x},\mathbf{u}) = \begin{bmatrix}
\frac{I_{b_1}}{\eta_1} \\
\frac{I_{b_2}}{\eta_2} \\
\frac{1}{C_c}\left(HG_1 + \frac{x_4 - x_3}{R_c}\right) \\
\frac{1}{C_s}\left(\frac{T_f - x_4}{R_u} - \frac{x_4 - x_3}{R_c}\right) \\
\frac{1}{C_c}\left(HG_2 + \frac{x_6 - x_5}{R_c}\right) \\
\frac{1}{C_s}\left(\frac{T_f - x_6}{R_u} - \frac{x_6 - x_5}{R_c}\right)
\end{bmatrix}, \qquad (8)
$$

$$
\begin{aligned}
\mathbf{v}_t = \mathbf{h}(\mathbf{x},\mathbf{u}) &= \begin{bmatrix} v_1 + I_{b_1} R_{0_1} & v_2 + I_{b_2} R_{0_2} \end{bmatrix}^T, \qquad (9) \\
I_{b_1} &= -I_{ch_1}(u_1, x_1) + I_{dis_2}(u_2, x_1, x_2) + I_e(t), \qquad (10) \\
I_{b_2} &= -I_{ch_2}(u_2, x_2) + I_{dis_1}(u_1, x_1, x_2) + I_e(t), \qquad (11)
\end{aligned}
$$

where $\mathbf{x} \in \Re^6$ is the state vector representing SoC of cell-1 (x_1) and cell-2 (x_2), the core and surface temperatures of cell-1 (x_3 and x_4) and the core and surface temperatures of cell-2 (x_5 and x_6), respectively. Moreover, u_i is the control vector representing the duty cycle of MOSFETs Q_1 and Q_2, respectively; I_e denotes the external current for a given drive cycle, η_i represents the scaling factors for SoC to current conversion, and C_c, C_s, R_c, and R_u are the thermal parameters defining the heat capacity of the cell core and surface, heat conduction resistance between the core and surface, and the convection resistance, respectively. HG_i represents the generated heat in cell i due to electrical and thermal actions, and T_f is the ambient temperature. The expression to calculate the heat generation term HG_i is given as:

$$
\begin{aligned}
HG_i &= -I_{b_i}(v_i - v_{t_i}) + (I_{b_i} T_i dU_i), \qquad (12) \\
T_1 &= \frac{x_3 + x_4}{2},\ T_2 = \frac{x_5 + x_6}{2},
\end{aligned}
$$

with T_i representing the average temperature of cell i in Kelvin. The temperature coefficient dU as a function of SoC is represented by the polynomial:

$$dU_i = \sum_{j=1}^{8} p_u x_i^{(8-j)}, \qquad (13)$$

with $p_u = [-125.8, 451.8, -637.1, 449.4, -166.5, 29.8, -1, -0.3]$ defining the polynomial coefficients. The SOC-OCV curve for the LFP-based battery is represented by a polynomial:

$$v_i = \sum_{j=1}^{9} p_{OCV_j} x_i^{(9-j)}, \tag{14}$$

where $p_{OCV} = [-413.1, 1938.9, -3744.2, 3856.1, -2293.9, 798.0, -157.1, 16.2, 2.5]$ represents the polynomial coefficients for the SOC-OCV relationship of the LFP cells.

III. Nonlinear Model Predictive Control of Active Cell Balancing

The NMPC is designed to yield an optimal solution for two competing objectives, i.e., increased balancing speed and reduced average temperatures of the cells. Therefore, the following nonlinear optimal control problem (NOCP) is formulated

$$\min_{\mathbf{x(k)},\mu(\mathbf{k})} J(\mathbf{x(k)}, \mu(\mathbf{k})), \tag{15}$$

$$J = \sum_{k=k_0}^{k_0+T_p} \Big(w_1(x_1 - x_2)^2 + w_2(T_1 - T_f)^2 + w_3(T_2 - T_f)^2 \Big),$$

subject to,

$$\mathbf{x(k+1)} - \mathbf{f}(\mathbf{x(k)}, \mu(\mathbf{k})) = 0, \tag{15a}$$

$$\mathbf{x}(k_0) = \mathbf{x}_{k_0}, \tag{15b}$$

$$\mu(\mathbf{k}) \in \mathcal{U}, \tag{15c}$$

$$\mathbf{x(k)} \in \mathcal{X}, \tag{15d}$$

$$\mu_1\mu_2 = 0,\ T_f \leq T_i \leq T_{max}, \tag{15e}$$

where $\mu(\mathbf{k}) = \mathbf{u(k)} - t_d/T$; T_p is the prediction horizon (s); $w_i \in \Re^+$ are the weights; x_{k_0} is the initial state vector and the sets $\mathcal{U}$ and $\mathcal{X}$ in (15c) and (15d), respectively are given as

$$\mathcal{U} = \left\{ \mu_i \in \Re^+ \middle| 0 \leq \mu_i \leq 0.3 - \frac{t_d}{T},\ \text{for } 1 \leq i \leq 2 \right\},$$

$$\mathcal{X} = \left\{ x_i \in \Re^+ \middle| x_{lb_i} \leq x_i \leq x_{ub_i},\ \text{for } 1 \leq i \leq 6 \right\}.$$

The equality and inequality constraints in (15e) ensure that both MOSFETs (cf. figure 1) are not turned on simultaneously, and average temperatures of both cells stay below the threshold temperature T_{max}.

The solution of the NOCP in (15) yields $\bar{\mathbf{x}}(k_0, k_0 + T_p)$, and $\bar{\mu}(k_0, k_0+T_p)$, and the closed-loop input for the interval $[k_0, k_0+T_p]$ is $\mu^* := \mu(k_0)$, whereas, the remaining elements $\mu(k_0 + 1, k_0 + T_p)$ are discarded.

IV. Results and Discussions

To verify the performance of the proposed ACBN, extensive simulation tests have been performed on a two-cell battery pack. The simulation framework includes both the electrical and thermal dynamics within the active cell balancing control architecture. The thermal model parameters for a 2.3 Ah A123 26650 $LiFePO_4$ battery are adapted from [16], and are presented in table I. Moreover, the electrical dynamics of a cell are modeled by a first-order ECM with the internal resistance R_0 taken as a function of the SoC and temperature. The relationship between cell SoC and OCV is fitted by a polynomial given by (14). Furthermore, the nominal model parameters used in the ACBN network are outlined in table II.

TABLE I: Electrical & Thermal model parameters

Parameter	Value	Units
C_s	4.5	JK^{-1}
C_c	62.7	JK^{-1}
R_c	1.94	KW^{-1}
R_u	3.19	KW^{-1}
η	2.3	Ah

TABLE II: Nominal model parameters of ACBN

Parameter	Value	Parameter	Value
T	20 μs	t_d	2 μs
V_F	0.3 V	R_{ds}	5.3 mΩ
t_f	8 ns	t_{rr}	28 ns
R_L	0.01 Ω	L	0.3 μH

The NMPC algorithm generates the duty cycle to control the switching of the buck-boost converter, with a particular emphasis on thermal management. The nonlinear optimal control problem (NOCP) is solved in MATLAB/Simulink through the CasADi toolbox, using the interior point optimizer (Ipopt) algorithm. The prediction horizon in the NMPC is taken as $T_p = 24$ s and the maximum temperature is taken as $T_{max} = 29.5$ C^0 in the constraint (15e). The robustness of the control scheme is evaluated under practical considerations such as: i) non-ideal resistances and capacities in the ACBN, ii) a generic highway current profile is taken as the input current to the battery pack with the magnitude of 1-C rate (2.3 A) as depicted in figure 5a, iii) R_0 is taken as a function of SoC and temperature in the ACBN network, however, R_0 takes 0.01Ω as a value in the NMPC iv) It is assumed that the initial cell temperatures within the battery pack are non-uniform, reflecting real-world scenarios where cells may not be at thermal equilibrium.

Various scenarios ranging from minimizing cell temperatures to prioritizing balancing speed are evaluated. Depending on w_i in (15), three different cases are considered for the cost function. The value of w_1 is selected as 10, 80 and 1000 in Case (a), Case (b) and Case (c), respectively. Whereas, $w_2 = w_3 = 1$ in Case (a) and Case (b), while in Case (c) $w_2 = w_3 = 0$.

The NMPC controller's performance, with its varying cost function weights, is presented in figures 3, 4, and 6. The analysis revealed that varying w_i in the NMPC's cost function significantly impacts the controller's behavior. Case (a), with its balanced approach, achieved moderate balancing times while maintaining temperatures close to T_f, ensuring both cell equalization and thermal safety. Case (b) prioritized SoC equalization, leading to a reduced balancing time at the expense of slightly higher temperatures. In contrast, Case

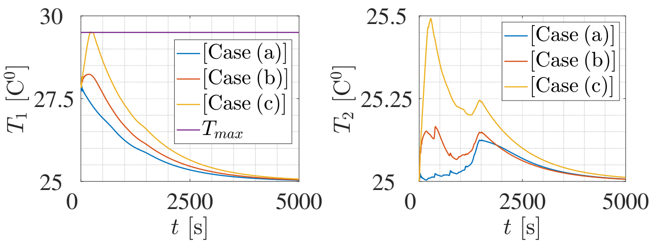

(a) Cell 1 temperature

(b) Cell 2 temperature

Fig. 3: Temperature responses of Cell 1 and Cell 2 in response to different cost function weights.

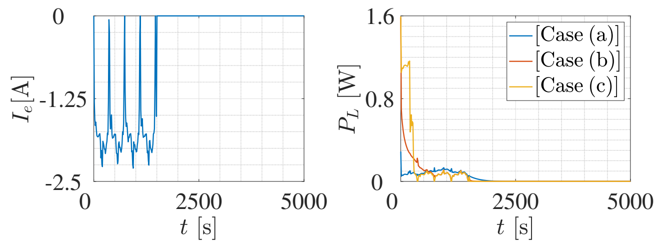

(a) Generic highway current profile

(b) Power losses

Fig. 5: Generic highway drive cycle and the influence of cost function weights on power losses

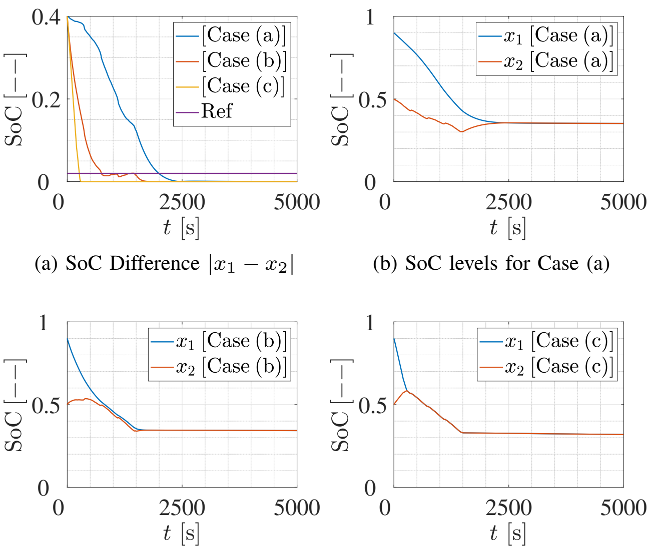

(a) SoC Difference $|x_1 - x_2|$

(b) SoC levels for Case (a)

(c) SoC levels for Case (b)

(d) SoC levels for Case (c)

Fig. 4: SoC Balancing performance of NMPC for various cost function scenarios.

(c), with its main focus on SoC balancing, resulted in the quickest balancing times but allowed the temperatures to increase without bounds. Luckily, the NPMC also includes thermal constraints that don't allow the temperature to rise beyond T_{max}, which is set to $29.5C^0$ in our case, as evident in the figure 3a.

The controller's performance in terms of cell balancing is depicted in figure 4, where cell SoCs are initialized at $[x_{1_0}\ x_{2_0}] = [0.9\ 0.5]$. The balancing performance is characterized in terms of the balancing time t_b, i.e., the time taken by the SoC difference to reach 0.02. The controller balances the SoC levels in $t_b = 1992s$ for Case (a), $t_b = 744s$ for Case (b) and $t_b = 264s$ for Case (c). Another important performance matrix is the average power loss $(\bar{P}_L)$ over the balancing time. The influence of cost function weights on the power losses is depicted in figure 5b. The average power losses are noted as $\bar{P}_L = 72.6mW$ in Case (a), $\bar{P}_L = 231.3mW$ in Case (b) and $\bar{P}_L = 989.8mW$ in Case (c). This result shows that the power losses are linked to the duty cycle and subsequently, the magnitude of balancing currents as depicted in figure 6. Higher balancing currents, as seen in Case (c), correspond to decreased balancing time but lead to elevated power losses due to increased electrical resistance heating within the cells. Furthermore, the thermal profiles of the cells, illustrated in figure 3, are directly influenced by these losses. The control input u_i, which dictates the charging and discharging currents of the buck-boost converter, thus plays a pivotal role in dictating the thermal behavior of each cell. A higher control input leads to a more substantial current flow, which, while achieving faster SoC balancing, also induces greater heat generation within the cells.

The above analysis highlights the trade-offs between balancing speed and thermal constraints. These scenarios illustrate the NMPC's diversity and its capability to adapt to different operational priorities as suited by the specific practical application. These results also highlight the importance of incorporating thermal dynamics into the cost function to manage battery temperatures effectively, which is crucial for safe battery operation and longevity.

V. Conclusions

This study presents a thermal management aware bi-directional active cell balancing network based on the NMPC for any two cells connected in series in a battery pack. The study incorporates a coupled electro-thermal model and a detailed model of the ACBN to account for the mean balancing currents and power losses. The robust NMPC framework meets the balancing objective and cell temperature regulation despite modeling uncertainties and a generic highway current profile. Simulation results confirm that the controller manages the trade-offs between balancing speed, power loss, and thermal regulation. Specifically, the results indicate that an emphasis on SoC balancing can lead to increased power losses and elevated cell temperatures. Conversely, incorporating temperature constraints within the NMPC cost function ensures thermal safety without significantly compromising on balancing performance. In conclusion, the developed control scheme successfully balances the competing objectives of SoC equalization and thermal management, providing a comprehensive solution for active cell balancing in battery packs.

Future work will expand the model to larger battery packs, validating the NMPC strategy with experimental data, inte-

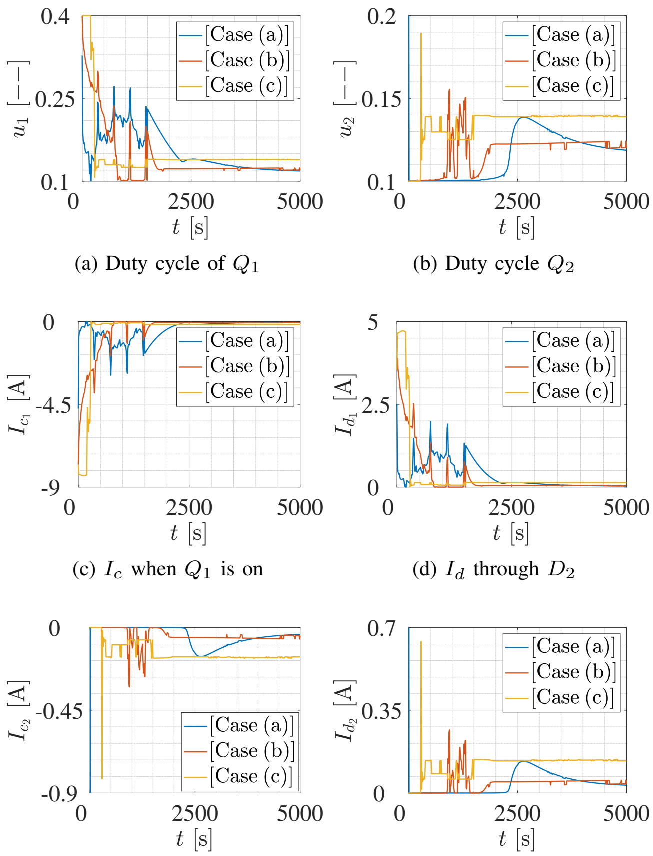

(a) Duty cycle of Q_1 (b) Duty cycle Q_2

(c) I_c when Q_1 is on (d) I_d through D_2

(e) I_c when Q_2 is on (f) I_d through D_1

Fig. 6: NMPC performance metrics comparison, duty cycle response, and balancing currents.

grate aging models for battery health, and develop strategies for EV range extension.

References

[1] F. S. J. Hoekstra, H. J. Bergveld, and M. C. F. Donkers, "Optimal control of active cell balancing: Extending the range and useful lifetime of a battery pack," *IEEE Transactions on Control Systems Technology*, vol. 30, no. 6, pp. 2759–2766, 2022.

[2] A. Pozzi, M. Zambelli, A. Ferrara, and D. M. Raimondo, "Balancing-aware charging strategy for series-connected lithium-ion cells: A nonlinear model predictive control approach," *IEEE Transactions on Control Systems Technology*, vol. 28, no. 5, pp. 1862–1877, 2020.

[3] J. Chen, A. Behal, and C. Li, "Active cell balancing by model predictive control for real time range extension," in *2021 60th IEEE Conference on Decision and Control (CDC)*, 2021, pp. 271–276.

[4] J. Liu, Y. Chen, and H. K. Fathy, "Nonlinear model-predictive optimal control of an active cell-to-cell lithium-ion battery pack balancing circuit," *IFAC-PapersOnLine*, vol. 50, no. 1, pp. 14 483–14 488, 2017, 20th IFAC World Congress.

[5] C. N. Van and T. N. Vinh, "Optimal Cell Equalizing Control Based on State of Charge Feedback for Lithium-ion Battery Pack," *International Journal of Control, Automation and Systems*, vol. 21, no. 5, May 2023. [Online]. Available: https://doi.org/10.1007/s12555-021-0648-1

[6] F. Hoekstra, H. Bergveld, and M. Donkers, "Range maximisation of electric vehicles through active cell balancing using reachability analysis," in *2019 American Control Conference (ACC)*, 2019, pp. 1567–1572.

[7] F. Hoekstra, L. W. Ribelles, H. Bergveld, and M. Donkers, "Real-time range maximisation of electric vehicles through active cell balancing using model-predictive control," in *2020 American Control Conference (ACC)*, 2020, pp. 2219–2224.

[8] S. M. Salamati, S. A. Salamati, M. Mahoor, and F. R. Salmasi, "Leveraging adaptive model predictive controller for active cell balancing in li-ion battery," in *2017 North American Power Symposium (NAPS)*, 2017, pp. 1–6.

[9] J. V. Barreras, C. Pinto, R. de Castro, E. Schaltz, S. J. Andreasen, and R. E. Araujo, "Multi-objective control of balancing systems for li-ion battery packs: A paradigm shift?" in *2014 IEEE Vehicle Power and Propulsion Conference (VPPC)*, 2014, pp. 1–7.

[10] J. V. Barreras, C. Pinto, R. de Castro, E. Schaltz, S. J. Andreasen, and R. E. Araújo, "Multi-objective control of balancing systems for li-ion battery packs: A paradigm shift?" in *2014 IEEE Vehicle Power and Propulsion Conference (VPPC)*. IEEE, 2014, pp. 1–7.

[11] Q. Ouyang, W. Han, C. Zou, G. Xu, and Z. Wang, "Cell balancing control for lithium-ion battery packs: A hierarchical optimal approach," *IEEE Transactions on Industrial Informatics*, vol. 16, no. 8, pp. 5065–5075, 2019.

[12] C. N. Van, "Optimal Control of Active Cell Balancing for Lithium-Ion Battery Pack With Constraints on Cells' Current and Temperature," *Journal of Electrochemical Energy Conversion and Storage*, vol. 20, no. 1, p. 011009, 05 2022. [Online]. Available: https://doi.org/10.1115/1.4054530

[13] V. Azimi, A. Allam, and S. Onori, "Extending life of lithium-ion battery systems by embracing heterogeneities via an optimal control-based active balancing strategy," *IEEE Transactions on Control Systems Technology*, vol. 31, no. 3, pp. 1235–1249, 2023.

[14] S. B. Javed, A. A. Uppal, M. R. Azam, K. Shehzad, and Q. Ahmed, "Model-based quantitative analysis of a capacitive cell balancing technique using soc estimator," in *2022 IEEE Conference on Control Technology and Applications (CCTA)*, 2022, pp. 670–675.

[15] A. A. Uppal, S. B. Javed, and Q. Ahmed, "Power losses aware nonlinear model predictive control design for active cell balancing," *IEEE Control Systems Letters*, vol. 7, pp. 3705–3710, 2023.

[16] X. Lin, H. E. Perez, S. Mohan, J. B. Siegel, A. G. Stefanopoulou, Y. Ding, and M. P. Castanier, "A lumped-parameter electro-thermal model for cylindrical batteries," *Journal of Power Sources*, vol. 257, pp. 1–11, 2014.